ELSEVIER

Journal of Structural Geology 30 (2008) 220–236

JOURNAL OF STRUCTURAL GEOLOGY

www.elsevier.com/locate/jsg

Complex deformation during arc–continent collision: Quantifying finite strain in the accreted Alisitos arc, Peninsular Ranges batholith, Baja California

H. Alsleben [a,*], P.H. Wetmore [b], K.L. Schmidt [c], S.R. Paterson [d], E.A. Melis [e]

[a] *Department of Geology, Texas Christian University, TCU Box 298830, Fort Worth, TX 76129, USA*
[b] *Department of Geology, University of South Florida, Tampa, FL 33620, USA*
[c] *Division of Natural Sciences, Lewis-Clark State College, Lewiston, ID 83501, USA*
[d] *Department of Earth Sciences, University of Southern California, Los Angeles, CA 90089, USA*
[e] *Department of Geological Sciences, University of Maine, Orono, ME 04469, USA*

Received 26 February 2007; received in revised form 23 October 2007; accepted 5 November 2007
Available online 12 November 2007

Abstract

The Early Cretaceous Alisitos island arc, located in the western part of the Peninsular Ranges batholith, Baja California, accreted to North America during the mid-Cretaceous. A syn- to post-collisional fold-thrust belt dominated by sinistral transpression and orthogonal convergence developed along the northern and eastern edges of the arc, respectively. Field observations across the fold-thrust belt show a deformation gradient with stronger planar and linear fabrics, fold tightening, and greater finite strain towards the arc–continent suture. Flattening strains dominate and finite strain intensity ranges from 0.08 to 2.71 and generally increases towards the suture. In detail, the fold-thrust belt narrows southward from ~12 km to ~3 km. Furthermore, finite strain is heterogeneous reflecting a heterogeneous fold-thrust belt characterized by local high strain zones near faults, folds, and igneous intrusions. Finite strain data and field observations allow several conclusions: (1) the colliding arc deformed significantly as a result of collision; (2) strain contributes to bulk shortening and crustal thickening in the collision zone; (3) geometry, composition, and tectonic setting of the continental margin prior to collision control along-strike variations in the fold-thrust belt; and (4) narrowing of the fold-thrust belt southward is offset by increased deformation in continental margin units.

Keywords: Peninsular Ranges batholith; Island arc collision; Fold-thrust belt; Finite strain; Crustal thickening; Bulk shortening

1. Introduction

The mid-Cretaceous suturing of the Alisitos island arc of Baja California (Fig. 1) to North America (e.g., Todd et al., 1988; Johnson et al., 1999a; Wetmore et al., 2002) left a superb geologic record of the collision between an arc and a continental margin. Arc accretion formed a fold-thrust belt that rims the arc along its northern and eastern margins. Along-strike changes in the structural character of the fold-thrust belt, which include the distribution of finite strain, and the mechanical behavior of the colliding arc are the focus of this paper.

Arc accretion was accommodated by sinistral transpression along the northern end of the Alisitos arc (Wetmore, 2003), where strong deformation affected arc strata to a distance of ~12 km southwest of the arc–continent suture, while orthogonal convergence dominated the east side of the arc (Johnson et al., 1999a; Schmidt and Paterson, 2002; Alsleben, 2005). Along the east side of the arc, the width of deformed arc strata narrows progressively southward from a 10-km wide zone to a <3 km wide zone at the southernmost study site, while continental margin units east of the arc record greater syn-collisional deformation southward. Furthermore, the presence of rheologically-strong units east of the Alisitos arc in the Sierra San Pedro Mártir (Fig. 1) resulted in significant ductile deformation in thermally weakened sediment-dominated

* Corresponding author. Tel.: +1 817 257 5455; fax: +1 817 257 7789.
E-mail address: h.alsleben@tcu.edu (H. Alsleben).

0191-8141/$ - see front matter © 2007 Elsevier Ltd. All rights reserved.
doi:10.1016/j.jsg.2007.11.001

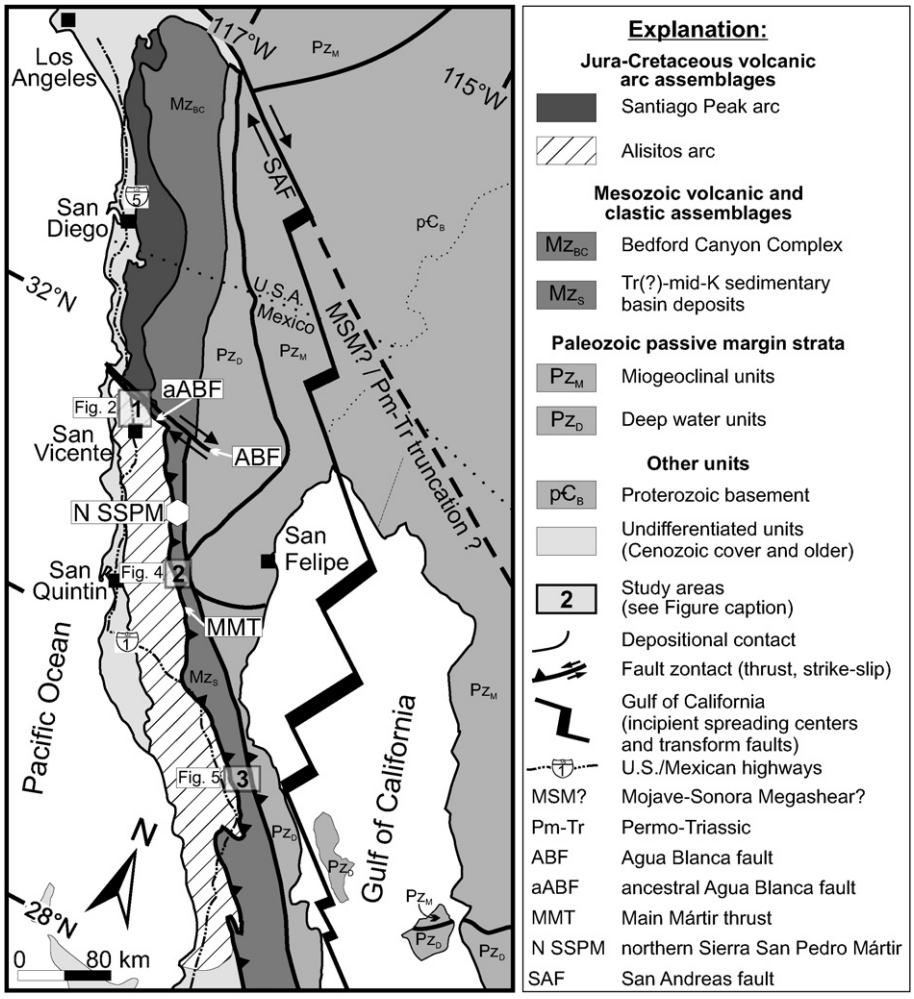

Fig. 1. Simplified geologic map of the Peninsular Ranges showing tectono-stratigraphic provinces. Boxes are study areas discussed in the text. 1, San Vicente area; 2, Southern Sierra San Pedro Mártir; 3, Sierra Calamajue.

assemblages (Schmidt and Paterson, 2002). Farther south in the Sierra Calamajue, where weaker assemblages dominate, deformation extends eastward into Paleozoic units (Campbell and Crocker, 1993; Alsleben, 2005).

Development of a fold-thrust belt suggests that fault displacement and rigid rotation by folding played significant roles during arc accretion. Furthermore, deformed markers indicate synchronous ductile deformation. Given the ductile deformation, we consider the importance of including strain-related data in the construction of balanced cross sections (e.g., Woodward et al., 1985; Mukul and Mitra, 1998), because without incorporating finite strain, shortening estimates in fold-thrust belts are minimum estimates.

Another issue that we consider is the spatial heterogeneity of finite strain. Causes for heterogeneity include primary fabrics (e.g., Paterson and Yu, 1994; Paterson et al., 1995) and clast-matrix competency contrasts (e.g., Hossack, 1968; Cobbold, 1977; Ramsay, 1982; Treagus, 1983; Treagus and Treagus, 2002), which produce different shape fabrics for the same bulk strain. Changes in environmental conditions (pressure, temperature, metamorphic fluids, and strain rate; e.g., Passchier and Trouw, 1996), local deformation gradients related to folding, faulting, and pluton emplacement, and regional along-strike variations in the tectonic setting, continental margin geometry, and geology can cause true finite strain variations and contribute to heterogeneity.

Below we introduce the Peninsular Ranges batholith (PRB) and the geology in the study areas. We then discuss the nature and distribution of finite strain in the Alisitos arc. Using these data, we estimate strain contributions to overall shortening and crustal thickening of the Alisitos arc. Finally, we discuss likely controls on the along-strike character of structures and finite strain in the collision zone and the mechanical behavior of the arc and continental margin during collision.

2. Geology of the Peninsular Ranges batholith (PRB)

Following the recognition of geologic E–W variations, the PRB, which includes Jura-Cretaceous batholithic rocks and Paleozoic–Mesozoic host strata (Fig. 1), was initially divided into three NW-trending basement assemblages (e.g., Gastil et al., 1975; Gastil, 1993). Recently Wetmore et al. (2002, 2003) recognized N–S variations and delimited two different arc segments. The northern segment is an in situ Cretaceous

continental margin arc (Santiago Peak arc) that unconformably overlies a Triassic–Jurassic accretionary prism (Bedford Canyon Complex) with North American affinities (e.g., Gehrels et al., 2002). In contrast, the southern segment is an accreted Cretaceous oceanic island arc (Alisitos arc) in fault contact with the arc to the north (Wetmore et al., 2002) and units to the east (Johnson et al., 1999a; Schmidt, 2000) (Fig. 1). Paleozoic North American passive-margin sequences subdivided into clastic deep-water assemblages and shallow-water carbonate-siliciclastic assemblages dominate the eastern PRB (Gastil and Miller, 1993).

The Alisitos arc, which is the main focus of this study, is commonly regarded as either a Cretaceous fringing island arc that formed following a Jurassic rifting event (e.g., Busby et al., 1998) or an exotic island arc that potentially formed a large distance from the North American margin and accreted to the continent after complete subduction of a separate oceanic plate (Johnson et al., 1999a). Beggs (1983) proposed a third alternative in which the Alisitos and Santiago Peak arcs, which were built on oceanic and continental crust, respectively, formed in a similar setting to the modern Aleutian arc (e.g., Fliedner and Klemperer, 2000). Although the origin of the Alisitos arc is debated, most workers agree that the arc was separated from the continent by an ocean basin of uncertain width during the Cretaceous (e.g., Busby et al., 1998; Johnson et al., 1999a; Wetmore et al., 2003). The collapse of this ocean basin, which began between ~115 and 110 Ma and was largely complete between 108 and 105 Ma, resulted in formation of a suture and fold-thrust belt that juxtaposes the Alisitos arc with North America. The suture has been named the ancestral Agua Blanca fault and Main Mártir thrust along the northern and eastern edge of the Alisitos arc, respectively (Johnson et al., 1999a; Wetmore et al., 2002).

3. Study areas

Studies of the fold-thrust belt geometry and finite strain were completed in the San Vicente area, the southern Sierra San Pedro Mártir, and the Sierra Calamajue (Fig. 1). Here, we summarize structural observations and present finite strain data from these areas, which are dominated by volcanic flows and breccias, pyroclastic deposits, volcanogenic argillites and sandstones, and carbonates. In addition, we completed reconnaissance finite strain analyses along the Main Mártir thrust in the northern Sierra San Pedro Mártir, which has been described in detail by Johnson et al. (1999a,b, 2003).

3.1. San Vicente area

The fold-thrust belt in the San Vicente area extends for ~5 km into the Santiago Peak arc and for ~12 km into the Alisitos arc, therefore reaching a total width of ~17 km (Fig. 2). Cretaceous Santiago Peak units retain depositional features such as accretionary lapilli and grading and are characterized by a series of kilometer-scale, WNW–ESE-trending, upright to overturned, close to tight folds, where both bedding and bedding-parallel foliation are folded (Wetmore, 2003). Sediment- and volcanic-dominated strata in the Alisitos arc show a well-developed spaced to continuous axial planar cleavage oriented subparallel to the trend of the fold-thrust belt (Wetmore, 2003). Multiple kilometer-scale, SW-vergent folds of bedding with varying tightness and subhorizontal fold axes are abundant. Folds show, from southwest to northeast, progressive tightening and overturning (Fig. 2). In addition, two larger (El Ranchito and El Tigre faults) and several smaller steeply NE-dipping, dominantly brittle faults with NE-side-up kinematics delimit several fault-bounded blocks. In contrast to these brittle structures, the ancestral Agua Blanca fault, which separates the Santiago Peak and Alisitos arcs, is a 50 to 100 m wide, WNW-trending, steeply NNE-dipping mylonitic ductile shear zone (Fig. 3a) that contains a steeply NE-plunging mineral stretching lineation (Wetmore et al., 2005). Asymmetric tails on sigma clasts in lineation-parallel sections suggest reverse (NE-side-up) shear, while clast shapes and folds in lineation-perpendicular sections also support an unconstrained amount of sinistral displacement. In the absence of detailed metamorphic petrology, outcrop observations suggest similar metamorphic conditions across the fold-thrust belt (Wetmore, 2003), which limits the cumulative amount of reverse shear on these steeply dipping faults to probably $\ll$ 5 km.

Deformed metasedimentary units with depositional ages between 117 and 110 Ma (inferred from detrital zircon data; Alsleben, 2005) are intruded by largely undeformed 108 to 105 Ma plutons that deflect and truncate regional structures (Fig. 2). These observations suggest that widespread deformation had ceased by this time (Wetmore, 2003). Subsequent shear became more localized as indicated by faults such as the ancestral Agua Blanca fault truncating and deforming the margins of a ~105 Ma Piedra Rodada pluton.

3.2. Southern Sierra San Pedro Mártir

In the southern Sierra San Pedro Mártir the fold-thrust belt trends NNW or ~50° clockwise with respect to the San Vicente area (Fig. 1). The area is located on the southwestern side of a ~20-km-wide doubly-vergent fan structure and is marked by a reverse metamorphic gradient and west-vergent reverse faults and mylonitic shear zones (Schmidt and Paterson, 2002). The arc strata are divided into western volcanic-dominated strata and eastern sediment-dominated units (Fig. 4) and are separated by the brittle-ductile Rosarito fault, which is characterized by steep, NE-dipping, spaced to locally penetrative cleavage, shear bands, and discrete chloritized fault surfaces with predominantly NE-over-SW kinematics. The Rosarito fault juxtaposes lithologies of similar metamorphic grade, whereas the Main Mártir thrust, which marks the eastern edge of the Alisitos arc, is a mylonitic shear zone that places continental margin strata over Alisitos arc strata and accommodated as much as 12 km of vertical displacement (Schmidt and Paterson, 2002). Deformation on these structures was on-going at ~101 Ma when the Rinconada pluton intruded (Fig. 4) and deformation halted by ~85 Ma as constrained by $^{40}Ar/^{39}Ar$ and apatite fission track studies (Schmidt, 2000).

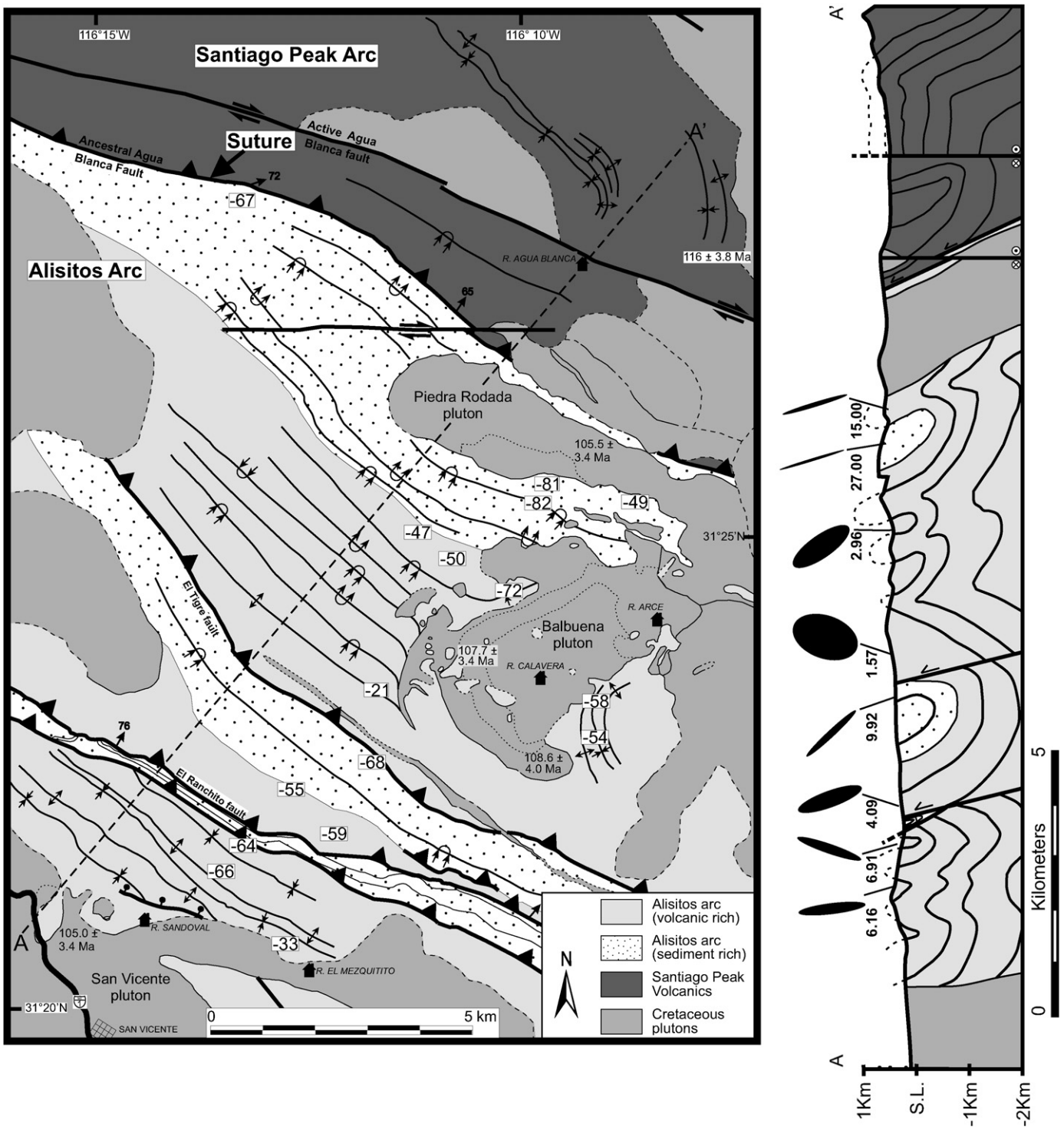

Fig. 2. Map showing basement units in the San Vicente area. Neogene cover has been removed. Strain sample locations are shown with shortening in the Z direction (where $X > Y > Z$) in percent. Cross section shows XZ strain ellipses and ratio for selected samples.

Arc and continental margin rocks exhibit dramatically different deformation styles and intensities (Schmidt and Paterson, 2002). Bedding of volcanic-rich assemblages is folded into map-scale open, upright folds with gently SE- and NW-plunging hinges. Immediately east of the Rosarito fault, folds tighten and fold axes plunge steeply and closer to the Main Mártir thrust folds are tight to isoclinal. Rock fabric intensities also increase from spaced- to continuous cleavage with a steeply-dipping stretching lineation. Across the Main Mártir thrust, folds are transposed by mylonite fabrics (Fig. 3b) that increase in intensity eastward and structurally upward, and ductile deformation takes up a significant portion of the shortening. Mylonitic lineations are dominantly NNE-trending, and s-c fabrics, asymmetric tails on sigma-clasts, and extensional

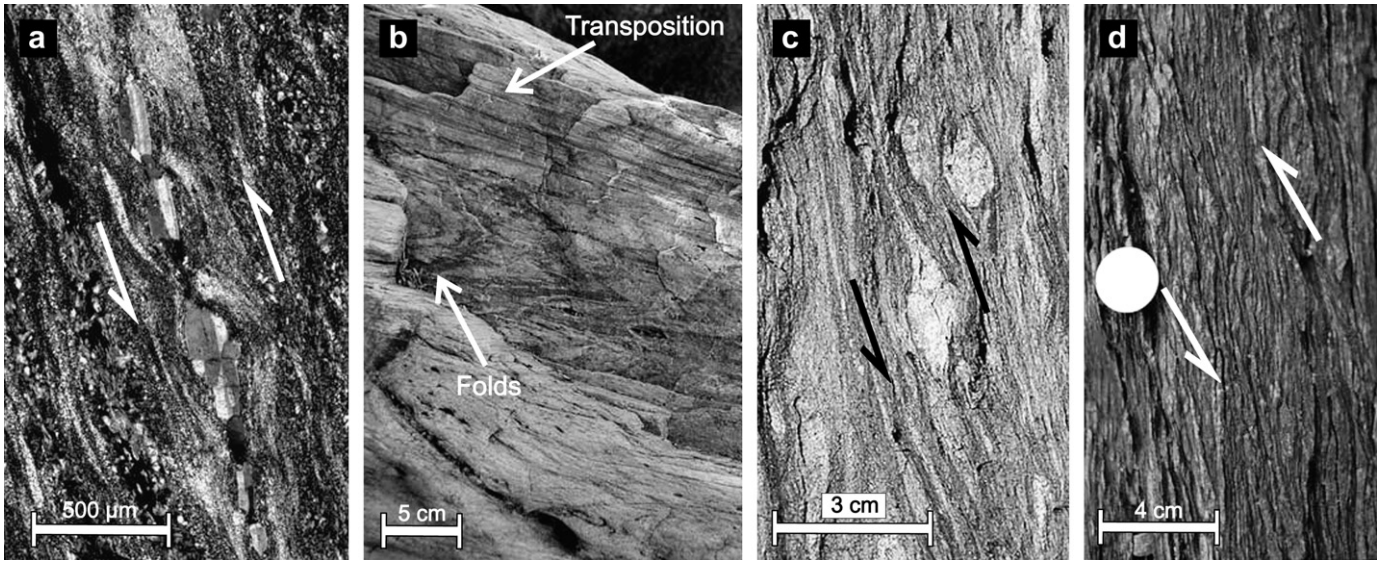

Fig. 3. Photographs showing some of the structures described in the text. (a) Photomicrograph (taken normal to foliation and parallel to lineation) of boudinaged plagioclase suggesting right-side up (to south-southwest) shear sense along the ancestral Agua Blanca fault. (b) Transposition of folds by shear along the Main Mártir thrust in the southern Sierra San Pedro Mártir. (c, d) Asymmetric lithic clast and s-c fabric from minor shear zones in the Sierra Calamajue showing right-side up (to southwest) kinematics.

crenulations show consistent NE-over-SW shear parallel to lineation.

3.3. Sierra Calamajue

The fold-thrust belt in the Sierra Calamajue (Fig. 1) is composed of units that are correlative with Alisitos arc volcanic-dominated assemblages, Mesozoic continental margin units, and Paleozoic deep-water passive margin sediments (Griffith and Hoobs, 1993; Schmidt and Paterson, 2002; Alsleben, 2005). These units are juxtaposed by reverse, NE-side-up faults as supported by kinematic indicators, such as tension cracks, asymmetric clasts (Fig. 3c), and s-c fabrics (Fig. 3d), and are internally faulted creating a number of fault-bounded blocks (Fig. 5). Brittle structures cross-cut earlier ductile structures throughout the area and faults may locally repeat section, but the lack of marker horizons and limited metamorphic changes, do not allow quantification of vertical offset across individual structures. The dominantly brittle character of the NW–SE striking, NE-dipping El Toro fault, which bounds the Alisitos arc and juxtaposes subgreenschist facies arc strata with greenschist facies continental margin strata, contrasts to the ductile deformation along the ancestral Agua Blanca fault and Main Mártir thrust farther north. However, narrow ductile shear zones exist in the area and reactivation of older ductile structures during late, brittle-slip events likely produced the observed relationships. The contact between greenschist facies continental margin units and overlying, lower-amphibolite facies Paleozoic units is the ductile to brittle El Molino fault (Fig. 5). Total vertical displacement across the fold-thrust belt is difficult to estimate, although the combined vertical displacement accommodated by these reverse faults may approach 5 or 6 km if metamorphic changes (Rothstein and Manning, 2003) are considered.

Deformation intensity increases from SW to NE across the fold-thrust belt. Gentle to open, outcrop-scale folds tighten from the southwest toward the El Toro fault. Increased fold tightening is accompanied by development of a NW–SE striking, moderately to steeply NE-dipping foliation with roughly down-dip mineral lineation. Northeast of the El Toro fault, folds remain tight and upright, and depositional features are increasingly obliterated. Across the El Molino fault, folds are overturned and SW-vergent (Fig. 5). Deformation in Paleozoic units involves at least one earlier phase of deformation unrelated to arc collision (Alsleben, 2005).

The minimum age for regional deformation in the Sierra Calamajue is constrained by Albian-Aptian fossils in arc strata (Griffith and Hoobs, 1993), a volcanic flow (TIMS U-Pb zircon age of ~125 Ma) in continental margin units (Griffith and Hoobs, 1993), and detrital zircon analyses that suggest a Cretaceous (~115 Ma) depositional age for continental margin turbidite sequences (Alsleben, 2005). A minimum age for initiation of deformation of ~115 Ma is inferred. Based on U-Pb zircon crystallization ages from the Las Palmas pluton (LA-ICPMS age; Fig. 5), which shows only weak magmatic fabrics, deformation ceased by ~95 Ma (Alsleben, 2005).

The geology in the Sierra Calamajue differs significantly from the Sierra San Pedro Mártir, despite their location along the east side of the Alisitos arc. In only the former, (1) deformation is locally concentrated in an ~6-km-wide fold-thrust belt; (2) brittle deformation resulted in complex faulting and slivering of all assemblages; (3) Alisitos arc strata record only limited deformation; (4) the metamorphic gradient is less severe; (5) Jurassic orthogneisses are not recognized; and (6) a fan structure did not develop.

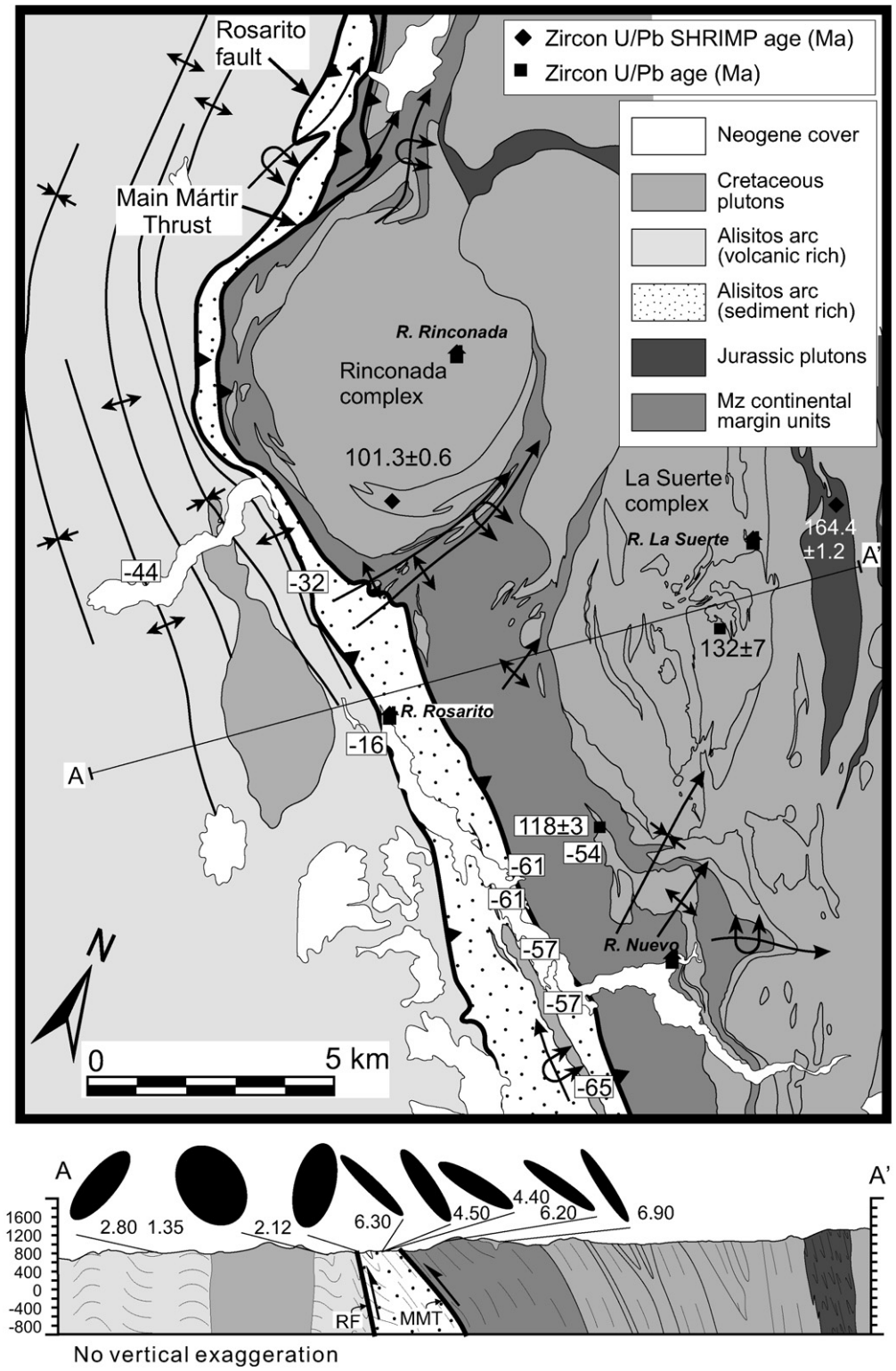

Fig. 4. Map of the southern Sierra San Pedro Mártir. Strain sample locations are shown with shortening in the Z direction (where $X > Y > Z$) in percent and cross section shows XZ strain ellipses and ratio for selected samples.

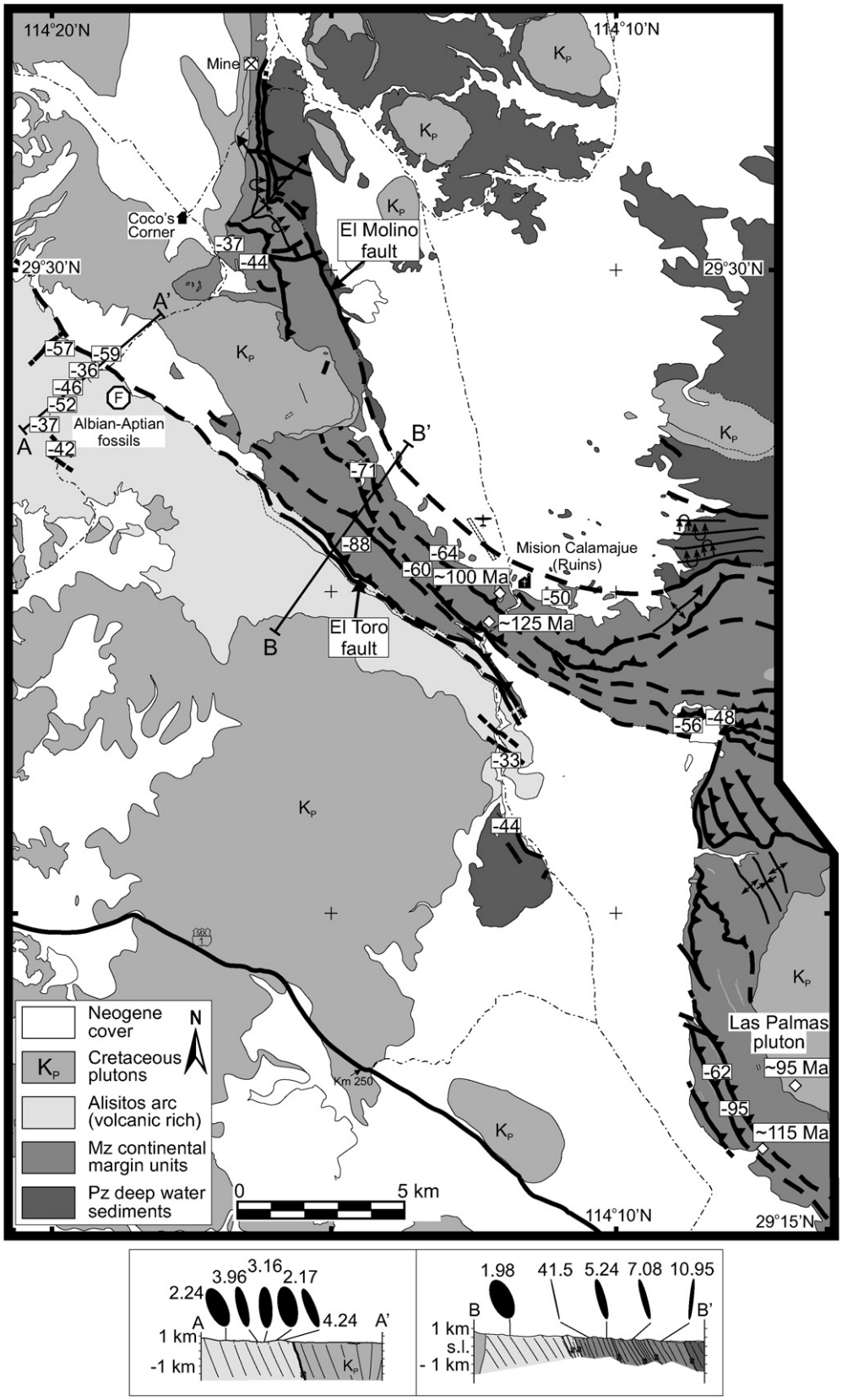

Fig. 5. Map of the Sierra Calamajue area. Strain sample locations are shown with shortening in the Z direction (where $X > Y > Z$) in percent and cross sections show XZ strain ellipses and ratio for selected samples.

4. Strain analyses

4.1. Introduction

We have compiled all published and unpublished finite strain analyses results of rheologically similar rock types (polymictic, lithic-rich volcaniclastics) from the Alisitos arc (Griffith and Hoobs, 1993; Chavez-Cabello, 1998; Johnson et al., 1999b; Schmidt, 2000; Wetmore, 2003; Alsleben, 2005) (Fig. 6; data tables are provided as supplementary material or can be requested from the principal author). In addition to data from the three study areas (described above), we included reconnaissance data from the Main Mártir thrust in the northern Sierra San Pedro Mártir (Johnson et al., 1999a). Data collected by others (Griffith and Hoobs, 1993; Chavez-Cabello, 1998; Johnson et al., 1999b) are shown in diagrams, but not described in detail.

4.2. Analytical procedure

Three mutually perpendicular, but otherwise arbitrary, cuts were made of each oriented sample and intersections were used to set up an *XYZ* coordinate system. On each face, the long and short axis (perpendicular to long axis) and the angle of the long axis relative to the reference frame were measured for 25 to 100 deformed markers. In each sample, we analyzed markers of similar composition, but size, composition, and matrix-clast ratios varied between samples. We avoided pumice clasts, which exhibit highly variable primary shapes (Tobisch et al., 1977; Wetmore, 2003). Using computer programs ''Strain'' (by S.R. Paterson et al., unpublished) and ''Rfphism'' (by M.T. Brandon; http://earth.geology.yale.edu/~brandon/Software/YALEDEFM/), which are based on algebraic solutions by Shimamoto and Ikeda (1976), two-dimensional strain ellipses, which represent mean aspect ratios and long-axis orientations for the measured marker population, were calculated. Standard errors, which were calculated by ''Rfphism'' using the bootstrap resampling method, for strain ratios range from 0.03 to 0.61 (average 0.15), whereas standard errors of long-axis orientations are between 0.4° and 28.8° (average 6.1°). Samples with smaller strain ratios generally record larger errors in long-axis orientations, whereas samples with greater strain ratios show larger aspect ratio errors. Three-dimensional fabric ellipsoids were calculated by the ''strain'' software from 2-D strain ellipses using the technique of Miller and Oertel (1979) and standard errors are generally <20%. These clast shape fabrics are unlikely to record bulk strain as clasts tend to be more competent than surrounding matrix (e.g., Treagus and Treagus, 2002). Although detailed data on competency contrasts are not available, the fabric data from clast populations of similar rock types can be used to determine the average strain for a particular lithology. These averages, however, may underestimate the whole-rock strain (Treagus and Treagus, 2002).

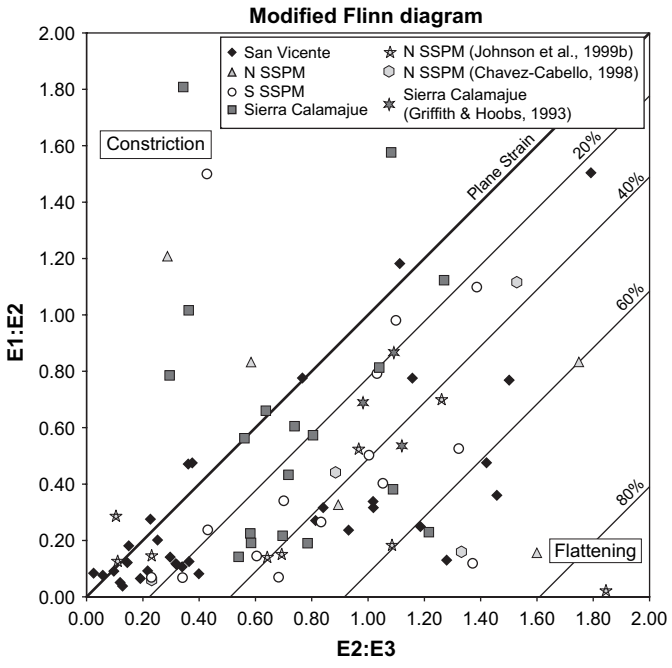

Fig. 6. Logarithmic Flinn diagram showing all available finite strain data ($n = 87$). Plane strain boundary lines are plotted for various percentages of volume change (after Twiss and Moores, 1992).

For each sample, assuming an initial random distribution of clast orientations and constant volume, the original length of the long (X), intermediate (Y), and short (Z) axes and the initial length ($l_o = (X \times Y \times Z)^{1/2}$) were calculated (see supporting material). These values allow calculation of elongations in percent (positive = lengthening, negative = shortening) and natural strains, which are the natural logarithms of the ratio for each axial length to the initial length [$E_1 = \ln(X/l_o)$; $E_2 = \ln(Y/l_o)$; $E_3 = \ln(Z/l_o)$]. Strain Intensity (SI) is equal to $1/\sqrt{3}\ [(E_1 - E_2)^2 + (E_2 - E_3)^2 + (E_1 - E_3)^2]^{1/2}$, where E_1, E_2, and E_3 are the principal natural strains (after Hossack, 1968). Symmetry is equivalent to the Lode's Parameter (LP) calculated from $[2(E_2) - E_1 - E_3]/[E_1 - E_3]$ where negative numbers are prolate shapes, zero equals plane strain, and positive numbers represent oblate shapes (Hossack, 1968).

4.3. Volume change

Examination of microtextures in thin sections cut close to the *XY* and *YZ* planes to assess stretch in the *Y*-direction and, therefore, volume change (cf. Yonkee, 2005) did not yield consistent results. Most examined samples displayed very short or no fibers in the *Y*-direction regardless of strain symmetry supporting no or only minor elongation consistent with no or small amounts of volume loss and a plane strain line through the origin of a Flinn diagram (Twiss and Moores, 1992). Locally longer fibers could be seen in samples with small (<0.5) k-values ($k = (R_{XY} - 1)/(R_{YZ} - 1)$; e.g., Ramsay, 1967) suggesting elongation in the *Y*-direction and possibly greater volume loss. Samples with large k-values lack clasts with well-developed seams or fibers at their ends, which would support shortening or extension in the *Y*-direction, respectively, and suggests no volume change for these samples. Additional complications arise from variations in fiber length

within individual samples, where longer fibers developed along some clasts, but no or only short fibers formed along others. Microtextural variations in the *Y*-direction and inconsistent relationships between microtextures and axial ratios prevent scaling principal stretches to estimate volume change (Yonkee, 2005), because the absolute stretch, which must be known for at least one direction (e.g., Barr and Coward, 1974), cannot be properly inferred from these observations. Based on microtextural observations, volume change might be variable on a microscopic scale and from sample to sample and is probably heterogeneous on a regional scale. However, the general lack of fibers or the presence of short fibers in the majority of the examined samples suggest no or only very limited volume change with the plane strain line crossing the Flinn diagram at the origin. Samples with low *k*-values potentially experienced an unconstrained amount of local volume loss. Volume loss estimates in similar rock types suggest volume losses of up to 25% (Bell, 1985; Boulter, 1986; Paterson et al., 1989), which would shift the plane strain line to the right of the origin (Twiss and Moores, 1992).

4.4. Summary of strain data

A Flinn diagram containing all data shows scatter (Fig. 6) indicating a complex strain field. Without considering potential volume changes, most data fall into the apparent flattening field, which is typical for fold-thrust belts (e.g., Hossack, 1968; Flöttmann and James, 1997; Mukul and Mitra, 1998; Kwon and Mitra, 2004). Although small analytical errors may contribute to the complexity of the pattern, those errors would not yield the observed scatter.

In the San Vicente area (Fig. 2), samples were collected from hinges and limbs of kilometer-scale folds, structural aureoles of intrusive bodies, hanging and footwalls of faults, areas distant to these structures, and also at a distance of ~25 km from the arc–continent suture. Strain intensity (SI) ranges from 0.08 to 2.3 (Fig. 7a–e). Samples collected ~25 km from the suture show low intensity ($SI < 0.2$), whereas strain intensity ranges from 0.3 to 2.3 in the ~12 km wide fold-thrust belt. Plane strain or minor volume loss are supported by microtextures, which show no or short fibers in the *Y*-direction at the end of lithic clasts. Volume loss might be associated with the ancestral Agua Blanca fault, where distinct fibers developed in the *Y*-direction. Dissolution seams, which would support shortening in the *Y*-direction have not been observed. In general, strain ellipsoid shapes range from plane to oblate strain and only samples with the smallest intensities exhibit prolate shapes (Fig. 6).

In the northern Sierra San Pedro Mártir (Fig. 1), analyses of five samples proximal to the Main Mártir thrust (≤1000 m; Fig. 7b) represent a limited dataset of thrust-related ductile strain, but data are insufficient to constrain regional ductile shortening quantitatively. Strain intensity varies from 0.9 to 1.9. Ellipsoid shapes range from oblate to prolate with Lode's parameters (LP) between −0.6 and 0.8 and microtextures show no distinct fibers in the *Y*-direction along clast ends, which supports plane strain conditions.

In the southern Sierra San Pedro Mártir, strain intensities qualitatively agree with observed rock fabrics (Schmidt, 2000). Greater strain intensity corresponds with strong ductile fabrics, and constrictional fabric symmetries are associated with strong lineation. Within ~500 m east and west of the Main Mártir thrust (Fig. 4), strain intensity ranges from 0.8 to 1.8 (Fig. 7c), which is comparable to values from the northern Sierra San Pedro Mártir (see above). Near the Rosarito fault, strain apparently drops significantly (SI 0.3 to 0.6), falling even lower a short distance farther west ($SI = 0.2$). This sharp strain drop is not supported by field observations of well-developed cleavage near the Rosarito fault, which could explain greater strain intensity (SI 0.75) ~3500 m west of the Main Mártir thrust. Strain symmetry ranges from mostly flattening fabrics (LP from 0.5 to 0.8) in rocks west of, and within, the Rosarito fault zone to more plane strain and constrictional fabrics (LP of −0.6) in rocks within the footwall and hanging wall of the Main Mártir thrust. Microtextures are variable and range from well-developed seams to distinct fibers in the *Y*-direction along clast ends. However, a clear relationship between microtextures and strain symmetry could not be established, indicating potentially heterogeneous volume change.

Strain intensity in the Sierra Calamajue generally increases toward the top of the section over a distance of ~3 km ranging from 0.5 to 2.7 (Fig. 7d). Alisitos arc strata record strain intensities from 0.5 to 1, whereas strain intensities range from 0.8 to 2.7 farther east into the fold-thrust belt. Strain in the area was close to plane strain as most samples, regardless of strain symmetry, showed either short or no fibers in the *Y*-direction and dissolution seams were not observed along clast ends. Strain samples plot in the flattening field or near plane strain and only two samples show apparent constrictional strains (Fig. 6).

Combining all data in a single plot reveals smallest strain intensities to the west and southwest of the suture (Fig. 7e). As folding and faulting intensifies closer to the suture, the strain increase is not linear with some of the greatest and least strain values measured near the suture, which supports an interpretation of a heterogeneous strain field and strain partitioning towards the suture. Furthermore, with few exceptions, microtextures support mostly no or very limited volume change and plane strain conditions.

4.5. Relationship between rock fabrics and strain ellipsoids

Although parallelism between strain axes and structural elements (*XY*-plane of the strain ellipsoid parallel to foliation and *X*-axis parallel to lineation) is an oversimplification (e.g., Bayly, 1974; Williams, 1976; Ramberg and Ghosh, 1977), several studies have validated these relationships (e.g., Ghosh, 1975; Williams, 1977). To assess these relationships in our dataset, strain samples were reoriented and geographic coordinates for strain ellipsoids were calculated (Fig. 8). Despite scatter in the dataset, average orientations of field data (Foliation: 314°/63°; $n = 33$; Lineation: 045°/63°; $n = 27$) are subparallel

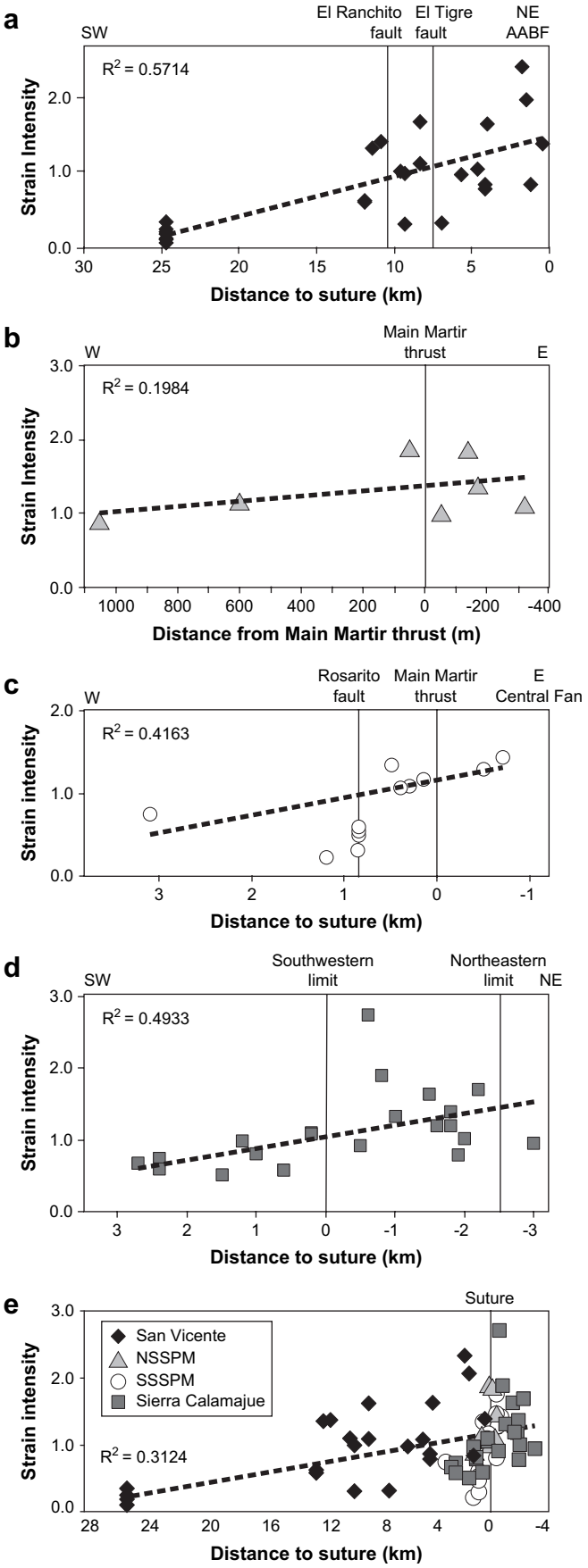

Fig. 7. Plots of strain intensity versus distance to the northern and eastern edges of the Alisitos arc. Note that horizontal and vertical scales vary between plots. (a) San Vicente area. (b) Near Main Mártir thrust in northern Sierra San Pedro Mártir. (c) Southern Sierra San Pedro Mártir. (d) Sierra Calamajue. (e) Combined data from all areas.

to average strain ellipsoid data (*XY*-plane: 322°/61°; $n = 33$; *X*-axes: 052°/62°; $n = 33$) suggesting parallelism between strain axes and structural elements on a regional scale.

4.6. Calculation of finite strain removal

Within each study area, finite strain fabrics, structural fabrics, and the trend of the fold-thrust belt are roughly subparallel. Using the program ''Meandefm'' (by M.T. Brandon), which calculates tensor averages from finite strain data using the Hencky method to account for directional changes of principal stretches (Brandon, 1995), we estimated the amount of arc perpendicular shortening and vertical extension by ductile strain across each study area (Table 1). These calculations require that averages apply to all rheologies. Although our sample density is limited and rock assemblages throughout the fold-thrust belt are heterogeneous, we argue that our estimates are conservative and probably underestimate the total finite strain. Volcanic units are likely rheologically stronger than sedimentary units and some lithic-rich volcanic units that contained extremely stretched markers could not be measured. Therefore, units, which experienced the largest amounts of strain, were not incorporated into these averages.

Further assumptions for strain removal include pure shear since shear zones with complex, possibly triclinic, fabric symmetry are rare, relatively narrow, and widely-spaced throughout the fold-thrust belt, and constant volume since microtextures do not unequivocally support volume changes. However, volume loss of up to 25% has been determined in similar rock types (Bell, 1985; Boulter, 1986; Paterson et al., 1989) and could affect these calculations. We retro-deformed a volume of rock whose horizontal dimensions equal the fold-thrust belt width as determined by mapping and a vertical dimension of 5 km (Table 1, Fig. 9), since field observations and limited thermo-barometry (Rothstein and Manning, 2003) suggest that those crustal levels are exposed. In the San Vicente area, a volume of rock that is $12 \times 12 \times 5\ km^3$ before strain removal, results in a volume of $22.2 \times 10.4 \times 3.6\ km^3$ (Table 1). For the southern Sierra San Pedro Mártir, where the fold-thrust belt in arc strata is ~10 km wide, we completed two calculations; one for sediment-dominated (~3 km wide) and one for volcanic-dominated (~7 km wide) sequences. Unstraining $3 \times 3 \times 5\ km^3$ in the former, results in a volume of $4 \times 2.6 \times 3.7\ km^3$, whereas the latter ($7 \times 7 \times 5\ km^3$) results in a volume of $8.9 \times 6.5 \times 4.2\ km^3$. In the Sierra Calamajue, we calculated separate values for the Alisitos arc and adjacent continental margin units. Each belt is ~3 km wide and after removing strain, the Alisitos arc is $3.6 \times 3 \times 4.2\ km^3$, whereas continental margin strata are $3.6 \times 2.7 \times 4.5\ km^3$.

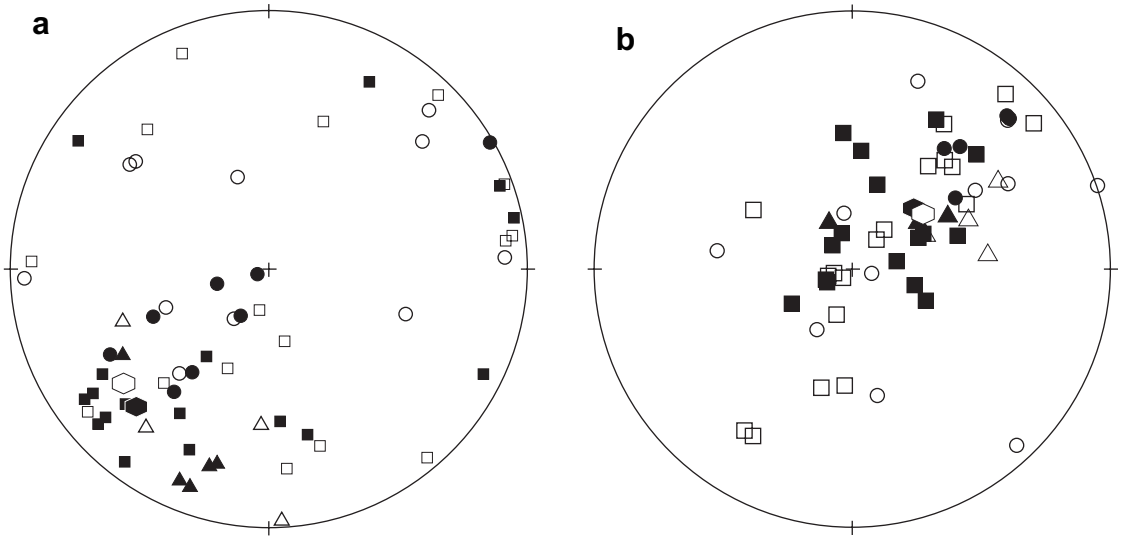

Fig. 8. Stereoplots showing field data and strain ellipsoid orientation data. a. Poles to foliation (closed symbols) and poles to XY plane of strain ellipsoid (open symbols). Triangle = Northern Sierra San Pedro Mártir; Circles = Southern Sierra San Pedro Mártir; Squares = Sierra Calamajue. Average orientation of foliation (closed hexagon): 314°/63° ($n = 33$); Average orientation of XY-plane (open hexagon): 322°/61° ($n = 33$). b. Plunge of lineation (closed symbols; average orientation (closed hexagon): 045°/63°; $n = 27$) and X-axes of strain ellipsoid (open symbols; average orientation (open hexagon): 052°/62°; $n = 33$). Shapes represent same areas as in a. Note that structural elements were not equally developed at all stations resulting in different numbers of data points.

5. Discussion

5.1. Deformation gradient and strain heterogeneity

Field observations and finite strain data support an east- and northeastward-increasing deformation gradient across the fold-thrust belt (Johnson et al., 1999a; Schmidt, 2000; Wetmore, 2003; Alsleben, 2005). These observations include: (1) gentle to open, upright folds on the west side of the arc that become gradually tighter and are nearly isoclinal adjacent to the suture (Johnson et al., 1999a; Schmidt, 2000; Wetmore, 2003); (2) rare ductile structures such as foliation or lineation on the west side of the arc outside of plutonic aureoles that are more common toward the suture, changing from a spaced cleavage that grades into continuous cleavage, and mylonitic fabrics in the Sierra San Pedro Mártir (Schmidt, 2000); and (3) gradual obliteration of depositional structures, which are well-preserved to the west and are increasingly overprinted and locally obliterated near the arc–continent suture. While ductile structures are better developed near the edge of the Alisitos arc, finite strain intensity also increases, although not linearly (Fig. 7).

In addition to the deformation gradient, several significant along-strike differences exist. For example, shear associated with the Main Mártir thrust in the Sierra San Pedro Mártir led to progressive rotation of fold hinges from gently plunging to down-dip, parallel to the direction of thrusting and resulted in juxtaposition of lower greenschist facies rocks in the footwall with amphibolite facies rocks in the hanging wall (Johnson et al., 1999a; Schmidt and Paterson, 2002). Shear of this magnitude is unlikely in the San Vicente area (Wetmore, 2003), where units record similar greenschist facies metamorphism, and the Sierra Calamajue (Alsleben, 2005), where metamorphic conditions across the suture change from sub-greenschist to greenschist facies conditions. Furthermore, shortening in the fold-thrust belt is accommodated by different structures. Folds dominate in the San Vicente area, whereas reverse faults are less common (Fig. 2; Wetmore, 2003). In contrast, narrow reverse shear zones and faults dominate in the Sierra Calamajue and kilometer-scale folds are less common (Fig. 5). In the Sierra San Pedro Mártir, contraction is accommodated by the Main Mártir thrust and abundant folds (Johnson et al., 1999a; Schmidt, 2000; Schmidt and Paterson, 2002).

To evaluate finite strain intensity and symmetry changes, we divided samples based on their proximity to folds, faults/shear zones, and pluton aureoles (Fig. 10). Based on field observations, samples located within 500 m of pluton margins or arc-bounding structures were considered in close proximity since this distance is qualitatively the maximum extent of emplacement- or shear-related strain. Shear-related strain is much narrower for minor shear zones or brittle faults within the fold-thrust belt and samples were considered proximal if they were collected within meters of faults/shear zones. All samples not located in pluton aureoles or near shear zones are located either in hinges or limbs of regional folds.

Scatter remains when samples are subdivided according to local strain setting (Fig. 10). One potential cause for the absence of emerging patterns is the superposition of primary fabrics ellipsoids, such as those determined from samples in the Alisitos arc located at distances >25 km from the suture (Fig. 10a), and tectonic strain ellipsoids, which will produce variations in the magnitudes and shapes of the finite strain ellipsoids (Paterson and Yu, 1994; Paterson et al., 1995; Wetmore, 2003). Furthermore, it is possible that the extent of shear zone- or emplacement-related strain is greater than anticipated and samples record strain related to multiple processes. Finally,

Table 1
Recalculation of finite strain data to horizontal shortening and vertical extension

	San Vicente	Southern SSPM		Sierra Calamajue	
	Alisitos (volcanics & sediments)	Alisitos volcanics	Alisitos sediments	Alisitos volcanics	Continental margin units
Tensor average *X*	41%	19%	53%	21%	12%
Tensor average *Y*	15%	8%	12%	0%	10%
Tensor average *Z*	−48%	−22%	−42%	−18%	−18%
Average foliation	297°/73°	n/a	322°/35°	318°/70°	318°/76°
Average lineation	72°/037°	n/a	37°/037°	70°/037°	75°/100°
Recalculation of strain to horizontal and vertical[a]					
Average *X*	39%	19%	32%	20%	12%
Average *Y*	15%	8%	12%	0%	10%
Average *Z*	−46%	−22%	−25%	−17%	−17%
Dimensions of unstrained rock volume ($Z \times Y \times X$)[b]	$12 \times 12 \times 5$ km^3	$7 \times 7 \times 5$ km^3	$3 \times 3 \times 5$ km^3	$3 \times 3 \times 5$ km^3	$3 \times 3 \times 5$ km^3
Z dimension after removing strain	22.2 km	8.9 km	4.0 km	3.6 km	3.6 km
Y dimension after removing strain	10.4 km	6.5 km	2.6 km	3 km	2.7 km
X dimension after removing strain	3.6 km	4.2 km	3.7 km	4.2 km	4.5 km
Arc perpendicular, horizontal shortening	10.2 km	1.9 km	1.0 km	0.6 km	0.6 km
Arc parallel extension	1.6 km	0.5 km	0.4 km	0 km	0.3 km
Crustal thickening	1.4 km	0.8 km	1.3 km	0.8 km	0.5 km

[a] Calculations assume that average foliation is equal to *XY*-plane of strain ellipsoid and mean lineation value is equal to *X*-axes of strain ellipsoid. Shortening and extension values are then taken to "unstrain" a volume of rock to pre-strain conditions. See Fig. 9 for graphic presentation.
[b] Z = dimension perpendicular to strike of fold-thrust belt; Y = dimension parallel to strike of fold-thrust belt; X = vertical crustal dimension.

our sampling density is probably too coarse to properly detect strain variations across individual folds, shear zones, and pluton aureoles (Fig. 10b–d). Finite strain variations are expected for individual folds since hinge- and limb-strains should vary according to the fold kinematic behavior (e.g., Ramsay, 1967; Ramsay and Huber, 1987). Similarly, finite strain variations and increases are expected to be non-linear towards the center of monoclinic shear zones (e.g., Ramsay, 1980) and structural aureoles of igneous intrusions (e.g., Gerbi et al., 2004). However, confirming finite strain variations associated with local deformation processes will require future work that gathers a set of samples specifically for analyzing the strain variation in individual folds, shear zones, and structural pluton aureoles.

Regardless of the scatter, available finite strain and age data allow preliminary strain rate estimates for the entire fold-thrust belt, but not each study area individually. Mid-Cretaceous (~115 Ma) volcanic flows (Carrasco et al., 1995; Johnson et al., 2003) and interlayered sedimentary units, which contain Albian fossils (Allison, 1955, 1974; Silver et al., 1963; Suarez-Vidal, 1987) and are thought to have been deposited by ~110 Ma (Wetmore, 2003; Alsleben, 2005), record widespread regional deformation. Deformation ceased between 108 and 105 Ma, as constrained by the age of the San Jose pluton in the northern Sierra San Pedro Mártir (Johnson et al., 2003) and Balbuena pluton in the San Vicente area (Fig. 2; Wetmore et al., 2005). Based on these constraints, finite strain accumulated over as little as 2 to 5 m.y. Using shortening estimates that range from 17% to 46% (Table 1), strain rates in the arc range from 1.08×10^{-15} s^{-1} to 7.29×10^{-15} s^{-1}. These estimates are at the low end of suggested regional strain rates in other orogenic belts, where rates range from 10^{-13} s^{-1} to 10^{-15} s^{-1} (e.g., Price, 1975; Pfiffner and Ramsay, 1982; Paterson and Tobisch, 1992; Müller et al., 2000).

5.2. Along-strike character of the fold-thrust belt

Deformation along the northern and eastern edges of the Alisitos arc suggests that the arc was not a rigid indenter, but accommodated significant internal deformation during collision. Internal deformation is concentrated in a southward narrowing fold-thrust belt that changes from ~12 km along the northern margin to ~10 km in the Sierra San Pedro Mártir to ~3 km in the Sierra Calamajue. Accompanying this width change are variations in the dominant shortening mechanisms, bulk shortening, and crustal thickening, which are controlled by (1) changes in the tectonic setting; (2) the pre-existing geometry of the continental margin; and (3) rheologic changes.

Wetmore (2003) estimated an average fold wavelength of ~1 km in the San Vicente area (Fig. 2). If the fold amplitude is ~$^1/_4$ the wavelength and using open to isoclinal fold morphologies (Wetmore, 2003), shortening estimates by folding reach as much as 50% in the area. In contrast, openly folded volcanic-rich strata in the southern Sierra San Pedro Mártir (Schmidt, 2000) record as little as ~15% fold-related shortening. This latter value could be significantly greater if shortening of isoclinally folded, mylonitic, sediment-rich Alisitos arc strata could be incorporated in these estimates. However, mylonitic fabrics almost completely transpose tight to isoclinal folds in the southern Sierra San Pedro Mártir (Fig. 3b) and it is not possible to properly account for fold-related shortening

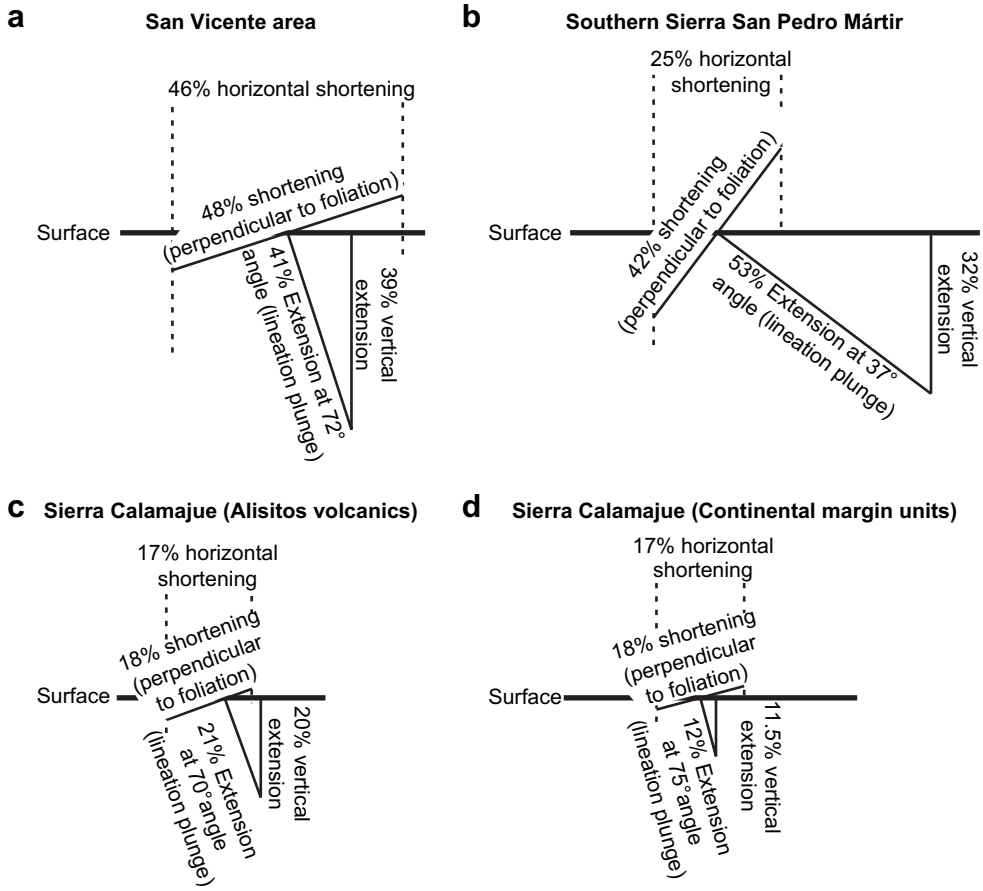

Fig. 9. Diagram explaining recalculation of finite strain shortening and extension values to horizontal shortening and vertical extension for all three study areas. Calculations assume that average foliation is equal to *XY*-plane of strain ellipsoid and mean lineation value is equal to *X*-axes of strain ellipsoid.

in these strata. In general, these constraints and changes from open to isoclinal geometries suggest that folding as a bulk shortening mechanism varies along- and across-strike of the fold-thrust belt and that fold-related shortening ranges from at least ~15% to ~50%.

First-order constraints of overall vertical fault displacements are established using petrologic observations and limited thermo-barometry data (e.g., Johnson et al., 1999a; Schmidt and Paterson, 2002; Rothstein and Manning, 2003; Wetmore, 2003; Alsleben, 2005; Melis, 2006). Throughout the Alisitos arc, greenschist-facies conditions dominate, which suggests minimal (≪5 km) vertical displacements across the fold-thrust belt. Metamorphic conditions do not change across the ancestral Agua Blanca fault into the Santiago Peak arc in the San Vicente area (Wetmore, 2003), which limits the amount of vertical displacement along this structure (≪5 km). In contrast, Al-in-hornblende barometry suggests an inverse metamorphic gradient and ~6 km (Melis, 2006) and possibly greater (Schmidt and Paterson, 2002) vertical displacement across the Main Mártir thrust in the Sierra San Pedro Mártir. Gradual eastward changes to lower amphibolite facies strata in the Sierra Calamajue support exhumation of somewhat deeper crustal levels (Rothstein and Manning, 2003) and cumulative vertical displacement between ~5 and 6 km, although not on the arc-bounding structure itself, which juxtaposes sub-greenschist facies arc strata with greenschist facies continental margin units. Obtaining better constraints is complicated by a lack of marker horizons and possible syn- to post-collisional rotation of faults and shear zones from gentle to now dominantly steep dips. Without these constraints, and with the exception of the Main Mártir thrust, which is a major contractional shear zone, faults caused only limited vertical displacements and bulk shortening associated with faulting was not significant either.

Contributions by finite ductile strain to arc perpendicular shortening and crustal thickening is greatest in the San Vicente area, where calculations across the ~12 km-wide fold-thrust belt in the Alisitos arc suggest up to 10 km shortening and 1.4 km of crustal thickening by penetrative ductile strain. Combining these calculations with fold-related shortening (up to 50% or 12 km), 22 km of bulk shortening is a first-order estimate. Similar calculations across Alisitos strata in the southern Sierra San Pedro Mártir yield arc-perpendicular shortening of 4 km (~1 km by folding and ~3 km by penetrative strain) and crustal thickening of ~1 km. Fold shortening estimates are not available for the Sierra Calamajue, but only 0.6 km of arc-perpendicular shortening and 0.8 km of crustal thickening are suggested across the 3-km-wide belt in the Sierra Calamajue (Table 1).

The variation in shortening magnitude can be attributed to geologic changes between the different study areas. Sinistral

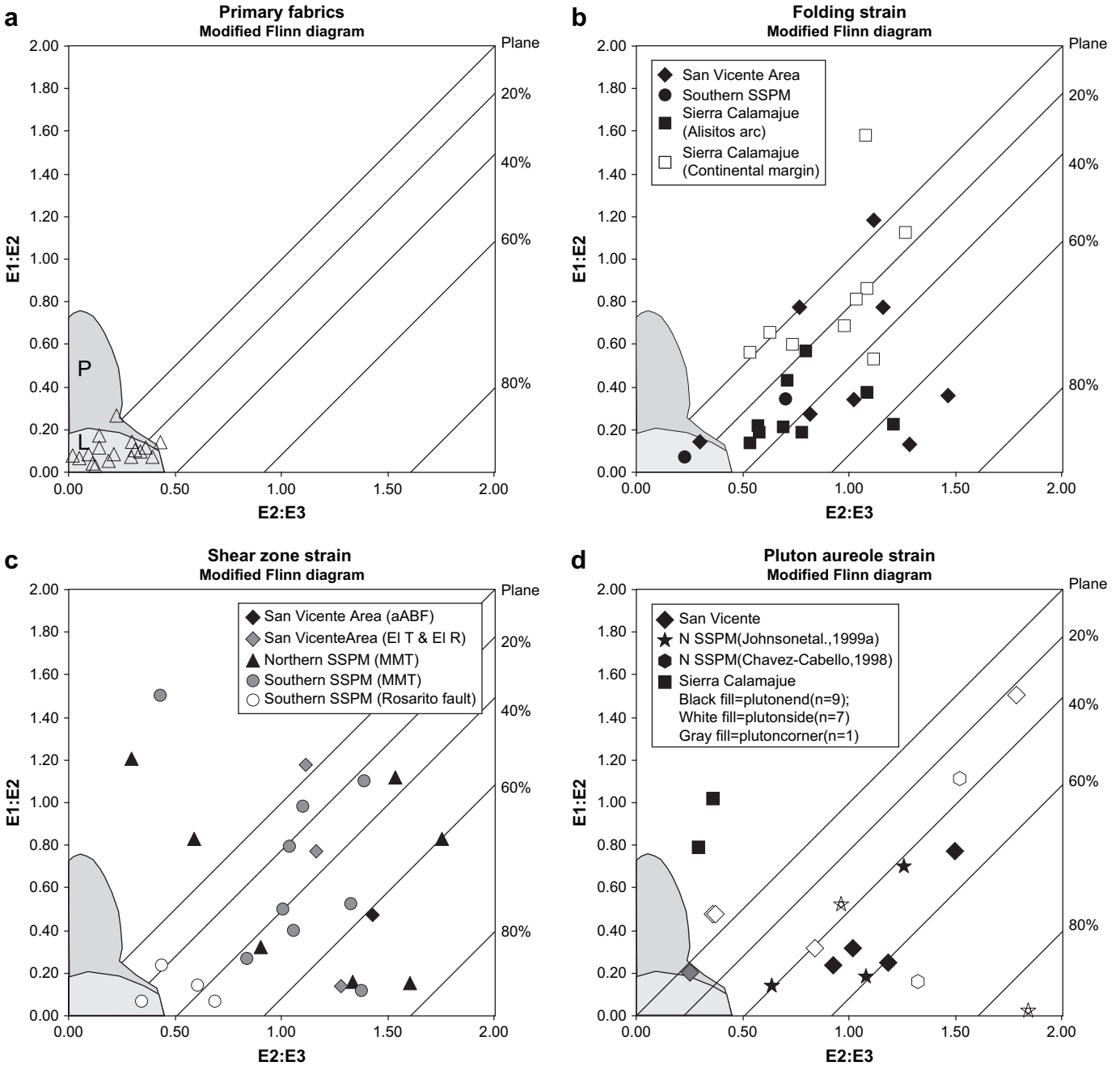

Fig. 10. Logarithmic Flinn diagrams showing data subdivided according to local strain setting. Figures include primary fabric fields for lithic-rich fragments (L) and phenocrysts (P) (after Wetmore, 2003). (a) Primary fabrics. (b) Fold-related strain. (c) Strain in shear zones. (d) Strain in pluton aureoles. aABF, ancestral Agua Blanca fault; El T, El Tigre fault; El R, El Ranchito fault; MMT, Main Mártir thrust; SSPM, Sierra San Pedro Mártir.

transpression and counter-clockwise rotation of structures along the northern edge of the Alisitos arc with respect to structures along the east side are expected for a colliding terrane that approaches from a westerly direction (Wetmore et al., 2002, 2003). A component of sinistral shear occurred along the ancestral Agua Blanca fault (Wetmore et al., 2002), whereas shortening is accommodated by the fold-thrust belt that stretches for ~17 km across the Alisitos and Santiago Peak arcs (Fig. 2). The concentration of deformation in the Alisitos arc is controlled by lithologic variations as submarine metasedimentary and metavolcanic strata of the Alisitos arc were likely rheologically weaker than dominantly subaerial metavolcanic rocks to the north. Furthermore, the Alisitos arc is younger (<116 Ma) and therefore potentially hotter and rheologically weaker than the Santiago Peak arc, which ranges from 128 to 116 Ma (e.g., Wetmore et al., 2003).

To the south, orthogonal convergence dominated along the east side of the arc (Johnson et al., 1999a; Schmidt, 2000; Alsleben, 2005), although Schmidt and Paterson (2002) could not discount limited (<10s of kilometers) sinistral, orogen-parallel shear within the core of the batholith east of the Main Mártir thrust. In the Sierra San Pedro Mártir, deformation

most strongly affected Alisitos arc strata that formed in marine basins along the east-side of the arc (e.g., Suarez-Vidal, 1987, 1993) and Jura-Cretaceous sheeted plutonic complexes in the central part of the PRB (Johnson et al., 1999a; Schmidt and Paterson, 2002). These units were sandwiched between the Alisitos arc to the west and a promontory of miogeoclinal carbonate strata to the east (Gastil, 1993), which acted as a rigid indenter (Fig. 1; Schmidt and Paterson, 2002). This geometry produced strong ductile deformation between these two entities, exhumation of mid-crustal strata, significant crustal thickening and ductile shortening (e.g., Johnson et al., 1999a), and formation of the doubly-vergent fan structure in the southern Sierra San Pedro Mártir (Schmidt and Paterson, 2002).

Farther south in the Sierra Calamajue, where the sediment-rich Alisitos arc strata are scarce, deformation was concentrated in Triassic through Cretaceous metasedimentary continental margin units and Paleozoic deep-water, shale-dominated units to the east of the arc (Campbell and Crocker, 1993; Alsleben, 2005). Thus, the arc volcanics to the west were rheologically stronger than continental margin and Paleozoic passive margin strata to the east. Collision of the arc resulted in more distributed deformation east of the arc and exhumation of shallower crustal levels than in the Sierra San Pedro Mártir. Thus, much of the deformation along the east-side of the Alisitos arc and adjacent continental margin units appears to be controlled by the kinematics of the collision (mostly orthogonal), margin geometry, and rheological character of the units involved in the collision.

6. Conclusions

Data and observations presented here allow several conclusions about the collision-related deformation in the Alisitos arc.

1. The strain field of the Alisitos arc is very heterogeneous and significant variations of strain magnitudes and ellipsoid shapes exist with most data lying in the apparent flattening field. The measured finite strain fabrics are controlled by primary fabrics, competency contrasts within the analyzed samples, changes in environmental conditions, and strain contributions from faulting, folding, and pluton emplacement.
2. Deformation in general and strain in particular increase from the west side of the arc, where samples record only primary fabrics, towards the suture zone that separates the Alisitos arc from the Santiago Peak arc to the north and North American continental margin strata to the east and strain tensor averages across the fold-thrust belt suggest between 17% and 46% arc-perpendicular ductile shortening.
3. Strain concentration along the northern and eastern edges of the Alisitos arc support a collision model for the arc with North America.
4. The arc did not behave as a rigid indenter. Collision-related deformation and the fold-thrust belt show along-strike variations whose characteristics are controlled by (a) the kinematic setting, which changes from sinistral transpression in the north to normal convergence along the eastern margin of the arc and is responsible for the counterclockwise deflection of structures in the northern Alisitos arc, (b) the pre-existing geometry of the continental margin, including an apparent promontory forming a rigid buttress at the latitude of the Sierra San Pedro Mártir, and (c) rheologic changes caused by the transition from miogeoclinal units east of the Sierra San Pedro Mártir to slope basin deposits east of the Sierra Calamajue and southward decrease of Cretaceous Alisitos arc-related sedimentary basin deposits.

Acknowledgments

This research was supported by National Science Foundation Grant EAR-97-8820 (S.R.P.), Geological Society of America Graduate Research Grants and Sigma Xi Grants-in-Aid of Research (H.A. and P.H.W.), and the Shackelford fund (P.H.W.). Reviews by Adolph Yonkee, an anonymous reviewer, and Bill Dunne helped improve the manuscript. Discussions with Greg Davis (USC) about Cordilleran tectonics and early comments on the manuscript by Scott Johnson (University of Maine) are gratefully acknowledged.

Appendix A. Supplementary data

Supplementary data associated with this article can be found, in the online version, at 10.1016/j.jsg.2007.11.001.

References

Allison, E.C., 1955. Middle cretaceous gastropoda from Punta China, Baja California, Mexico. Journal of Paleontology 29, 400–432.

Allison, E.C., 1974. The type Alisitos Formation (Cretaceous, Aptian-Albian) of Baja California and its bivalve fauna. In: Gastil, G., Lillegraven, J. (Eds.), A Guidebook to the Geology of Peninsular California. AAPG, Pacific Section, pp. 20–59.

Alsleben, H., 2005. Changing characteristics of deformation, sedimentation, and magmatism as a result of island arc-continent collision. Ph.D. thesis, University of Southern California.

Barr, M., Coward, M.P., 1974. A method for the measurement of volume change. Geological Magazine 111, 293–296.

Bayly, B.M., 1974. Cleavage not parallel to finite-strain ellipsoids *XY*-Plane: discussion. Tectonophysics 23, 205–208.

Beggs, J.M., 1983. Stratigraphy, petrology, and tectonic setting of the Alisitos Group, Baja California, Mexico. Ph.D. thesis, University of California, Santa Barbara.

Bell, A., 1985. Strain paths during slaty cleavage formation—the role of volume loss. Journal of Structural Geology 7, 563–568.

Boulter, C.A., 1986. Accretionary lapilli-filled clastic dykes: a comparison of compaction strain estimates from dyke folding and lapilli shape factors. Journal of Structural Geology 8, 201–204.

Brandon, M.T., 1995. Analysis of geologic strain data in strain-magnitude space. Journal of Structural Geology 17, 1375–1385.

Busby, C., Smith, D., Morris, W., Fackler-Adams, B., 1998. Evolutionary model for convergent margins facing large ocean basins: Mesozoic Baja California, Mexico. Geology 26, 227–230.

Campbell, M., Crocker, J., 1993. Geology west of the Canal de Las Ballenas, Baja California, Mexico. In: Gastil, R.G., Miller, R.H. (Eds.), The Pre-Batholithic Stratigraphy of Peninsular California. GSA Special Paper, 279, pp. 61–76.

Carrasco, A.P., Kimbrough, D.L., Herzig, C.T., 1995. Cretaceous arc-volcanic strata of the western Peninsular Ranges: comparison of the Santiago Peak Volcanics and Alisitos Group. Abstracts of III Peninsular Geological Society International Meeting.

Chavez-Cabello, G., 1998. Ascent mechanisms, emplacement and magmatic evolution of several plutons located on the western side of the Sierra San Pedro Mártir, Baja California, Mexico. M.S. Thesis, CICESE, Ensenada, Mexico.

Cobbold, P.R., 1977. Description and origin of banded deformation structures. Canadian Journal of Earth Sciences 14, 1721–1731.

Fliedner, M.M., Klemperer, S.L., 2000. Crustal structure transition from oceanic arc to continental arc, eastern Aleutian Islands and Alaska Peninsula. EPSL 179, 567–579.

Flöttmann, T., James, P., 1997. Influence of basin architecture on the style of inversion and fold-thrust belt tectonics–the southern Adelaide Fold-Thrust Belt, South Australia. Journal of Structural Geology 19, 1093–1110.

Gastil, R.G., 1993. Prebatholithic history of peninsular California. In: Gastil, R.G., Miller, R.H. (Eds.), The Prebatholithic Stratigraphy of Peninsular California. GSA Special Paper, 279, pp. 145–156.

Gastil, R.G., Miller, R.H., 1993. The Prebatholithic Stratigraphy of Peninsular California. GSA Special Paper 279.

Gastil, R.G., Phillips, R., Allison, E., 1975. Reconnaissance geology of the State of Baja. GSA Memoir 140.

Gehrels, G.E., Stewart, J.H., Ketner, K.B., 2002. Cordilleran-margin quartzites in Baja California—Implications for tectonic transport. EPSL 199, 201–210.

Gerbi, C., Johnson, S.E., Paterson, S.R., 2004. Implications of rapid, dike-fed pluton growth for host-rock strain rates and emplacement mechanisms. Journal of Structural Geology 26, 583–594.

Ghosh, S.K., 1975. Distortion of planar structures around rigid spherical bodies. Tectonophysics 28, 185–208.

Griffith, R., Hoobs, J., 1993. Geology of the southern Sierra Calamajue, Baja California Norte, Mexico. In: Gastil, R.G., Miller, R.H. (Eds.), The Prebatholithic Stratigraphy of Peninsular California. GSA Special Paper, 279, pp. 43–60.

Hossack, J.R., 1968. Pebble deformation and thrusting in the Bygdin area (Southern Norway). Tectonophysics 5, 315–339.

Johnson, S.E., Tate, M.C., Fanning, C.M., 1999a. New geologic mapping and SHRIMP U-Pb zircon data in the Peninsular Ranges Batholith, Baja California, Mexico; evidence for a suture? Geology 27, 743–746.

Johnson, S.E., Paterson, S.R., Tate, M.C., 1999b. Structure and emplacement history of a multiple-center, cone-sheet-bearing ring complex: The Zarza intrusive complex, Baja California, Mexico. GSA Bulletin 111, 607–619.

Johnson, S.E., Fletcher, J.M., Fanning, C.M., Paterson, S.R., Vernon, R.H., Tate, M.C., 2003. Structure and emplacement of the San Jose tonalite pluton, Peninsular Ranges batholith, Baja California, Mexico. Journal of Structural Geology 25, 1933–1957.

Kwon, S., Mitra, G., 2004. Strain distribution, strain history, and kinematic evolution associated with the formation of arcuate salients in fold-thrust belts; the example of the Provo Salient, Sevier Orogen, Utah. In: Sussman, A.J., Weil, A.B. (Eds.), Integrating Paleomagnetic and Structural Analyses. GSA Special Paper, 383. Orogenic Curvature, pp. 205–223.

Melis, E.A., 2006. Structural, temporal, and metamorphic evolution of the Main Mártir thrust, Baja California, Mexico. Ph.D. thesis, University of Maine.

Miller, D.M., Oertel, G., 1979. Strain determination from the measurement of pebble shapes: a modification. Tectonophysics 55, T11–T13.

Müller, W., Aerden, D., Halliday, A.N., 2000. Isotopic dating of strain fringe increments; duration and rates of deformation in shear zones. Science 288, 2195–2198.

Mukul, M., Mitra, G., 1998. Finite strain and strain variation analysis in the Sheeprock thrust sheet; an internal thrust sheet in the Provo salient of the Sevier fold-and-thrust belt, central Utah. Journal of Structural Geology 20, 385–405.

Passchier, C.W., Trouw, R.A.J., 1996. Microtectonics. Springer, Berlin, Germany.

Paterson, S.R., Tobisch, O.T., 1992. Rates of processes in magmatic arcs: implications for the timing and nature of pluton emplacement and wall rock deformation. Journal of Structural Geology 14, 291–300.

Paterson, S.R., Yu, H., 1994. Primary fabric ellipsoids in sandstones: implications for depositional processes and strain analysis. Journal of Structural Geology 16, 505–517.

Paterson, S.R., Tobisch, O.T., Bhattacharyya, T., 1989. Regional, structural and strain analyses of terranes in the western Metamorphic Belt, central Sierra Nevada, California. Journal of Structural Geology 11, 255–273.

Paterson, S.R., Yu, H., Oertel, G., 1995. Primary and tectonic fabric intensities in mudrocks. Tectonophysics 247, 105–119.

Pfiffner, O.A., Ramsay, J.G., 1982. Constraints on geological strain rates; arguments from finite strain states of naturally deformed rocks. Journal of Geophysical Research 87, 311–321.

Price, N.J., 1975. Rates of deformation. Journal Geological Society London 131, 553–575.

Ramberg, H., Ghosh, S.K., 1977. Rotation and strain of linear and planar structure in three-dimensional progressive deformation. Tectonophysics 40, 309–337.

Ramsay, J.G., 1967. Folding and Fracturing of Rocks. McGraw-Hill, New York.

Ramsay, J.G., 1980. Shear zone geometry: A review. Journal of Structural Geology 2, 83–99.

Ramsay, J.G., 1982. Rock ductility and its influence on the development of tectonic structures in mountain belts. In: Hsue, K.J. (Ed.), Symposium on Mountain Building: Mountain Building Processes. Academic Press, London.

Ramsay, J.G., Huber, M.I., 1987. Techniques of Modern Structural Geology: Folds and Fractures. Academic Press, London.

Rothstein, D.A., Manning, C.E., 2003. Geothermal gradients in continental magmatic arcs: Constraints from the eastern Peninsular Ranges batholith, Baja California, México. In: Johnson, S.E., Paterson, S.R., Fletcher, J.M., Girty, G.H., Kimbrough, D.L., Martin-Barajas, A. (Eds.), Tectonic Evolution of Northwestern Mexico and the Southwestern United States. GSA Special Paper, 374, pp. 337–354.

Schmidt, K.L., 2000. Investigations of arc processes: relationships among deformation magmatism, mountain building, and the role of crustal anisotropy in the evolution of the Peninsular Ranges batholith, Baja California. Ph.D. thesis, University of Southern California.

Schmidt, K.L., Paterson, S.R., 2002. A doubly-vergent fan structure in the Peninsular Ranges batholith: Transpression or local complex flow around a continental margin buttress? Tectonics 21 (5), 1050, doi:10.1029/2001TC001353.

Shimamoto, T., Ikeda, Y., 1976. A simple algebraic method for strain estimation from deformed ellipsoidal objects. 1. basic theory. Tectonophysics 36, 315–337.

Silver, L.T., Stehli, G.G., Allen, C.R., 1963. Lower Cretaceous pre-batholithic rocks of northern Baja California, Mexico. AAPG Bulletin 47, 2054–2059.

Suarez-Vidal, F., 1987. The calcareous facies of the Alisitos formation, evidence for an early Cretaceous tectonic calm. Ciencias Marinas 13, 131–154.

Suarez-Vidal, F., 1993. The Aptian-Albian on the west coast of the state of Baja California, a mixture of marine environments. In: Abbott, P.L., Sangines, E.M., Rendina, M.A. (Eds.), Geologic Investigations in Baja California, Mexico. South Coast Geological Society, pp. 125–138.

Tobisch, O.T., Fiske, R.S., Sacks, S., Taniguchi, D., 1977. Strain in metamorphosed volcaniclastic rocks and its bearing on the evolution of orogenic belts. GSA Bulletin 88, 23–40.

Todd, V.R., Erskine, B.G., Morton, D.M., 1988. Metamorphic and tectonic evolution of the northern Peninsular Ranges batholith, southern California. In: Ernst, W.G. (Ed.), Metamorphism and Crustal Evolution of the Western United States, Rubey Volume VII. Prentice-Hall, pp. 894–937.

Treagus, S.H., 1983. A theory of finite strain variation through contrasting layers, and its bearing on cleavage refraction. Journal of Structural Geology 5, 351–368.

Treagus, S.H., Treagus, J.E., 2002. Studies of strain and rheology of conglomerates. Journal of Structural Geology 24, 1541–1567.

Twiss, R.J., Moores, E.M., 1992. Structural Geology. W.H. Freeman, New York.

Wetmore, P.H., 2003. Investigation into the tectonic significance of along strike variations of the Peninsular Ranges batholith, southern and Baja California. Ph.D. thesis, University of Southern California.

Wetmore, P.H., Schmidt, K.L., Paterson, S.R., Herzig, C., 2002. Tectonic implications for the along-strike variation of the Peninsular Ranges Batholith, Southern and Baja California. Geology 30, 247–250.

Wetmore, P.H., Herzig, C., Alsleben, H., Sutherland, M., Schmidt, K.L., Schultz, P.W., Paterson, S.R., 2003. Mesozoic tectonic evolution of the Peninsular Ranges of southern and Baja California. In: Johnson, S.E., Paterson, S.R., Fletcher, J.M., Girty, G.H., Kimbrough, D.L., Martin-Barajas, A. (Eds.), Tectonic Evolution of Northwestern Mexico and the Southwestern United States. GSA Special Paper, 374, pp. 93–116.

Wetmore, P.H., Alsleben, H., Paterson, S.R., Ducea, M.N., Gehrels, G.E., Valencia, V.A., 2005. Field trip to the northern Alisitos arc segment: Ancestral Agua Blanca fault region. Field Conference Guidebook, Peninsular Geological Society VII International Meeting, Ensenada, MX.

Williams, P.F., 1976. Relationship between axial plane foliations and strain. Tectonophysics 30, 181–196.

Williams, P.F., 1977. Foliation: a review and discussion. Tectonophysics 39, 305–328.

Woodward, N.B., Boyer, S.E., Suppe, J., 1985. An outline of balanced cross-sections. University of Tennessee Department of Geological Sciences, Knoxville, TN.

Yonkee, A., 2005. Strain patterns within part of the Willard thrust sheet, Idaho-Utah-Wyoming thrust belt. Journal of Structural Geology 27, 1315–1343.